4Pi-Confocal Imaging in Fixed Biological Specimens

Martin Schrader,* Karsten Bahlmann,* Günter Giese,# and Stefan W. Hell*
*High Resolution Optical Microscopy Group, Max Planck Institute for Biophysical Chemistry, D-37070 Göttingen, and #Max Planck Institute for Cell Biology, D-68526 Ladenburg, Germany

ABSTRACT By combining the wavefronts produced by two high-aperture lenses, two-photon 4Pi-confocal microscopy allows three-dimensional imaging of transparent biological specimens with axial resolution in the 100–140-nm range. We reveal the imaging properties of a two-photon 4Pi-confocal microscope as applied to a fixed cell. We demonstrate that a fast, linear point deconvolution suffices to achieve axially superresolved 3D images in the cytoskeleton. Furthermore, we describe stringent algorithms for alignment and control of the two lenses. We also show how to compensate for the effects of a potential refractive index mismatch of the mounting medium with respect to the immersion system.

INTRODUCTION

A major advantage of far-field light microscopes, such as confocal and multiphoton microscopes, over their near-field counterparts is their unique capability to produce three-dimensional (3D) images of the interior of cells. Unfortunately, the resolution of these systems is limited to 200 nm and 500–900 nm in the lateral and axial directions, respectively. Mathematical restoration of the images (Agard and Sedat, 1983; Carrington et al., 1995; Kano et al., 1996; Loew et al., 1993; Van der Voort and Strasters, 1995) can improve the resolution up to a factor of 2–3, provided that the signal-to-noise ratio is high and the effective point-spread function (PSF) of the microscope is well known. A recent review of 3D microscopy is given in the volumes by Sheppard and Shotton (1997) and Pawley (1995) and the references therein.

4Pi-confocal microscopy is a 3D-fluorescence technique for improving axial resolution (Hell and Stelzer, 1992; Schrader and Hell, 1996) by physical means. In type A 4Pi-confocal microscopy this is achieved by coherently illuminating the same object point in the sample with two opposing lenses of high numerical aperture. Coherent superposition of the two focused wavefronts increases the overall aperture of the system. In the case of constructive interference, the focal axial intensity distribution is governed by a main maximum and one pronounced lobe on each side. The main maximum is about three to four times narrower than that of a single lens, reflecting its potential for superresolution. The lobes, however, carry the risk of producing artifacts in the image. For unambiguous 3D imaging, their effect must be suppressed. Two-photon excitation in conjunction with confocal detection reduces the height of the lobes. For a typical excitation wavelength $\lambda = 800$ nm, the full width at half-maximum (FWHM) of the main maximum is ~145 nm, and the lobes are ~25–45% of the height of the main maximum. The lobes can be removed after (or even during) image acquisition by means of a linear point deconvolution (Hänninen et al., 1995). As a result, an effective 3D-PSF consisting of a single spot of ~250 nm lateral and 145 nm axial FWHM is achieved.

Interference of counterpropagating unfocused waves has been used in standing-wave microscopy (SWM) to increase axial resolution (Bailey et al., 1993; Lanni, 1986). However, SWM and 4Pi-confocal microscopy differ considerably in their approaches to increasing resolution, in their imaging properties, and in their PSF. The SWM is based on a conventional microscope and relies on flat counterpropagating waves, which, for constructive interference, results in a maximum that is accompanied by about three lobes on either side. The first lobes are ~80% of the total main maximum, because suppression by two-photon excitation and confocalization is not possible in a SWM. The simultaneous presence of several lobes of 80–120-nm axial distance requires the specimens to be almost equally thin or sparse to provide unambiguous axial separation (Freimann et al., 1997). Nevertheless, the SWM is a very useful instrument, because it allows fast data acquisition and provides an overview in the conventional nonscanning mode. Within the uncertainty given by the periodicity, the SWM can discern structures that are 50–120 nm apart. On the other hand, the strength of 4Pi-confocal microscopy is the spatially defined 3D-PSF allowing for defined imaging in three dimensions.

In its earliest stages, 4Pi-imaging in a cell was considered challenging (Lindek et al., 1994). Recently, however, the applicability of this technique to image cellular filamentous actin has been shown, albeit only in combination with a maximum likelihood estimation (MLE) restoration algorithm restoring the 4Pi data with the 4Pi-PSF (Hell et al., 1997). The combination of two-photon excitation 4Pi-confocal microscopy and restoration has revealed an unprecedented 3D resolution in the 100-nm range (Hell et al., 1997).

Received for publication 2 March 1998 and in final form 22 June 1998.

Address reprint requests to Dr. Stefan Hell, High Resolution Optical Microscopy Group, Max Planck Institute for Biophysical Chemistry, D-37070 Gottingen, Germany. Tel.: 49-551-2011366; Fax: 49-551-2011085; E-mail: shell@gwdg.de.

Dr. Giese's present address is MPI for Medical Research, Department of Molecular Cell Research, D-69120 Heidelberg, Germany.

0006-3495/98/10/1659/10 $2.00

The axial lobe removal was also implicitly performed by the MLE algorithm.

Although powerful, restoration algorithms still have the inherent drawback of requiring extensive, off-line computations. To a certain extent, nonlinear restoration techniques are object dependent, i.e., the sparse and thinner objects converge better and faster in the restoration procedure. Here we demonstrate that the fast, simple, one-dimensional, and linear point deconvolution is mostly sufficient for obtaining axially superresolved 4Pi images of biological samples. This is demonstrated by directly comparing two-photon excitation 4Pi-confocal images of type A with two-photon confocal images of filamentous actin of fibroblast cells.

Furthermore, we discuss the optical conditions to be met to successfully apply 4Pi-confocal microscopy to superresolution cellular imaging. We elaborate on the effect of a mismatched refractive index of the sample and the immersion system and demonstrate how to compensate for it. We also describe the alignment and control of the two objective lenses, which is important for ensuring a good overlap of the two coherent light fields in a 4Pi-confocal arrangement.

ONLINE SIDE-LOBE REMOVAL IN 4Pi-CONFOCAL IMAGES

The effective PSF of a confocal fluorescence microscope is the product of the excitation PSF, $h_{\mathrm{ill}}(r, z) = |\vec{E}(r, z)|^2$, where $\vec{E}$ is the normalized electric field in the focal region of the objective lens, and the detection PSF, $h_{\mathrm{det}}(r, z)$, which approximates well to the excitation PSF calculated at the fluorescence wavelength (Wilson and Sheppard, 1984):

$$h(r, z) = h_{\mathrm{ill}}(r, z) \cdot h_{\mathrm{det}}(r, z) \tag{1}$$

In the 4Pi arrangement (Fig. 1), the PSF of illumination is obtained by the coherent summation of two focused fields (Hell and Stelzer, 1992):

$$h^{\mathrm{ill}}_{4\mathrm{Pi}}(r, z) = |\vec{E}_1(r, z) + \vec{E}_2(r, z)|^2 \tag{2}$$

Near doubling of the excitation wavelength increases the spatial extent of the 4Pi illumination PSF by a factor of 2; two-photon excitation renders an excitation PSF proportional to the square of the illumination intensity in the focus. Thus, in combination with confocal detection, the two-photon 4Pi-confocal PSF (of type A) is given by

$$h_{4\mathrm{Pi(A)}} \approx |h^{\mathrm{ill}}_{4\mathrm{Pi}}(r/2, z/2)|^2 \cdot h_{\mathrm{det}}(r, z) \tag{3}$$

Two-photon excitation combined with confocal detection reduces the lobes by twofold. First, the squared dependence of the fluorescence on the illumination intensity reduces the excitation efficiency at lower intensity regions. Second, the spatially broader illumination PSF, $h^{\mathrm{ill}}_{4\mathrm{Pi}}$, pushes the side lobes away from the focal plane, where they are subject to stronger suppression by the confocal pinhole. In theory this combination should render lobes of only 8–14% (Hell et al., 1994). However, longitudinal chromatic and spherical aberrations compromise this effect, so that in practice a lobe of 25–50% on either side of the main maximum is encountered.

The 4Pi-confocal PSF is sketched in Fig. 2 *a* (*left*), and, in general terms, can be regarded as the convolution of a single peak function (Fig. 2 *a*, *center*) and a lobe function (Fig. 2 *a*, *right*) describing the location and the relative height of the lobes. Thus it is possible to obtain a single peak by deconvoluting the PSF with the inverse of the lobe function. This procedure is carried out along the optic axis, line by line for each *x*-*y* coordinate in the plane. According to standard imaging theory, the image is given by the convolution of the unknown object function with the PSF. Hence one can cancel the effect of the lobes by deconvoluting the complete image or 3D data set with the inverse function of the lobe function (Hänninen et al., 1995), line by line along *z*. The result is an image, the resolution of which is determined solely by the sharp main maximum of the 4Pi-confocal PSF.

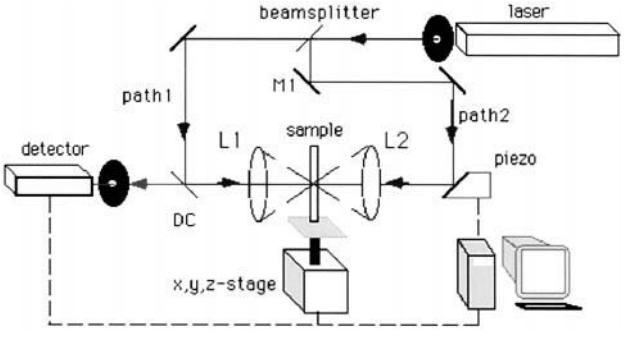

FIGURE 1 Setup of a 4Pi-confocal microscope of type A, featuring illumination through two opposing objective lenses L_1 and L_2 and confocal detection.

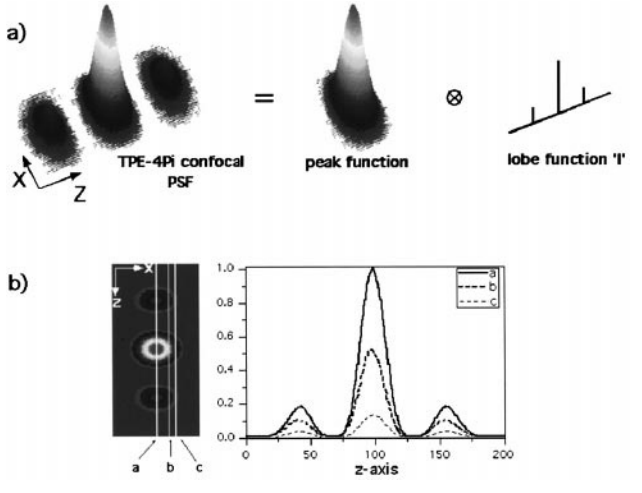

FIGURE 2 (*a*) Sketch of a two-photon 4Pi-confocal PSF of type A as a convolution of a single peak function and a lobe function. (*b*) Comparison of axial intensity profiles of a two-photon 4Pi-confocal PSF at different lateral distances to the optical axis.

Point deconvolution differs radically from familiar "deconvolution" or restoration methods by not requiring the full mathematical description of the PSF. Instead it merely uses the location and the relative height of the two lobes. Being a one-dimensional operation using a discrete function consisting of a few points, point deconvolution is fast and can be carried out online during 4Pi image acquisition.

For point deconvolution to be applicable, two conditions must be fulfilled. First, the relative height of the side lobes must not depend on a lateral offset with respect to the axis (Fig. 2 *b*). Second, the PSF has to be spatially invariant in the image. While the latter condition is a general requirement for all deconvolution techniques, the first one is only inherent in point deconvolution of 4Pi-confocal images. The validity of the first condition can be verified by comparing axial profiles (along the *z* axis) through the PSF at different lateral positions (*xy*). On the right side of Fig. 2 *b*, three *Z*-profiles through a theoretical two-photon excitation 4Pi-confocal PSF are displayed. The relative heights of the side lobes along the indicated lines are (*line a*) 17.5%, (*line b*) 18.6%, and (*line c*) 24.2%, indicating that the relative heights of the lobes increase slightly with lateral defocus. However, at line c, for example, the height of the PSF has already dropped below 15%, so this variation introduces an absolute error of less than 2%, which is usually below the noise level. This allows the use of a one-dimensional point deconvolution without significant introduction of artifacts.

The constancy of the relative height of the lobes with lateral offset can also be derived from the two-photon 4Pi-confocal optical transfer function (Gu and Sheppard, 1994). An intuitive explanation is the fact that the two-photon confocal PSF is of nonlinear nature (see Eq. 3). In a sense, the two-photon confocal PSF is related to a third-order power dependence on local intensity, with two orders stemming from the two-photon excitation and another order from the multiplication with the confocal detection. (In a single-photon confocal or in a three-photon confocal microscope, this would be second and fourth order, respectively.) The third-order dependence of the effective PSF suppresses the outer parts (i.e., the secondary maxima) of the PSF, which eventually leads to relative constancy of the lobes with respect to the main maximum. It is important to realize that in the PSF of a conventional microscope the relative height of the secondary maxima increases with lateral defocus. In an axial profile the side maxima and therefore interference-produced lobes would gain weight in the profile and even outweigh the main maximum. An axial profile that resembles constructive interference in the center of the PSF may well appear "destructive" when laterally defocused. This is the intuitive reason why the production of a single sharp maximum by point deconvolution should work only in 4Pi-confocal microscopy but not in a conventional microscopy-based, standing-wave microscope. Before demonstrating the usefulness of point deconvolution in the recording of 4Pi images within a cell, we would like to address another important reason for the successful application of 4Pi-confocal microscopy in cellular imaging, namely the counteraction of the refractive index mismatch-induced phase shift.

REFRACTIVE INDEX MISMATCH-INDUCED PHASE CHANGES AND THEIR COMPENSATION

4Pi microscopy requires that the relative phase of the two spherical wavefronts in the image be strictly constant, or at least that its change be well understood. In cases of significant mismatch between the sample refractive index and the immersion system, the relative phase changes with the axial position of the scanning focus. Let n_1 and n_2 be the refractive index of the immersion system and the sample, respectively. Fig. 3 illustrates that the optical path from the exit pupil of the objective lens to the common focal point depends on the axial position of the sample. When the sample is being axially scanned to the right, the length of the optical path at the left-hand side will increase, whereas that on the right will decrease if $n_1 > n_2$, and vice versa. The result is a change in the relative phase of the two interfering beams and therefore a change in the position and height of the interference maxima in the PSF. A typical example of this is a specimen that is mounted in glycerol and investigated under a microscope with an oil immersion objective lens.

We investigated the effect of index mismatch on the relative phase in a microscope by recording images from mouse skin fibroblasts. The cells grown on a microscopic coverslip were fixed as described elsewhere (Bacallao et al., 1990) and stained for F-Actin content by using phalloidin-tetramethyl rhodamine isothiocyanate (phalloidin-TRITC) (P-5157; Sigma, Deisenhofen, Germany). The samples were mounted on identical coverslips in a small drop of a 1:1 (v/v) mixture of glycerol and vectashield (Vector, Burlingame, CA). The refractive index of the embedding medium was 1.46. The resulting coverslip sandwiches were sealed with fingernail polish. Fig. 4 shows a large area overview of the sample recorded in a standard single-photon confocal microscope.

Fig. 5 demonstrates the effect of the index mismatch on the relative phase. It shows an axial section through one of the fibroblasts of Fig. 4, but this time recorded with a type

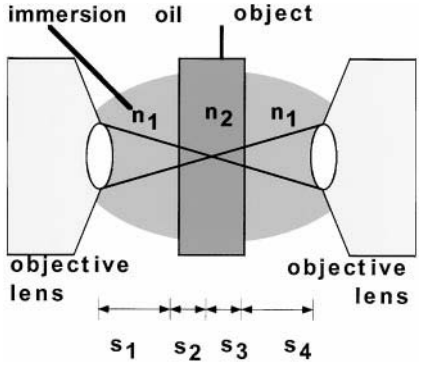

FIGURE 3 The optical paths through immersion oil and sample.

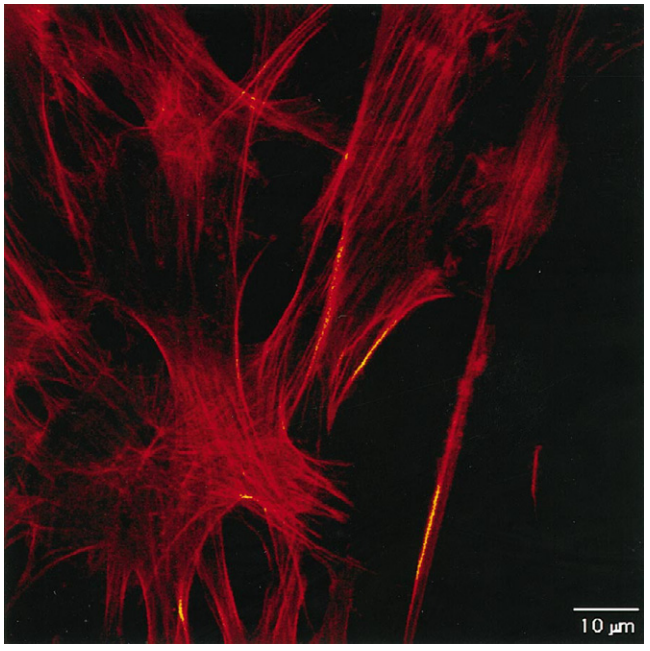

FIGURE 4 Confocal fluorescence *x-y* overview image of mouse skin fibroblast cells labeled for filamentous actin, taken with a commercial single-photon confocal microscope.

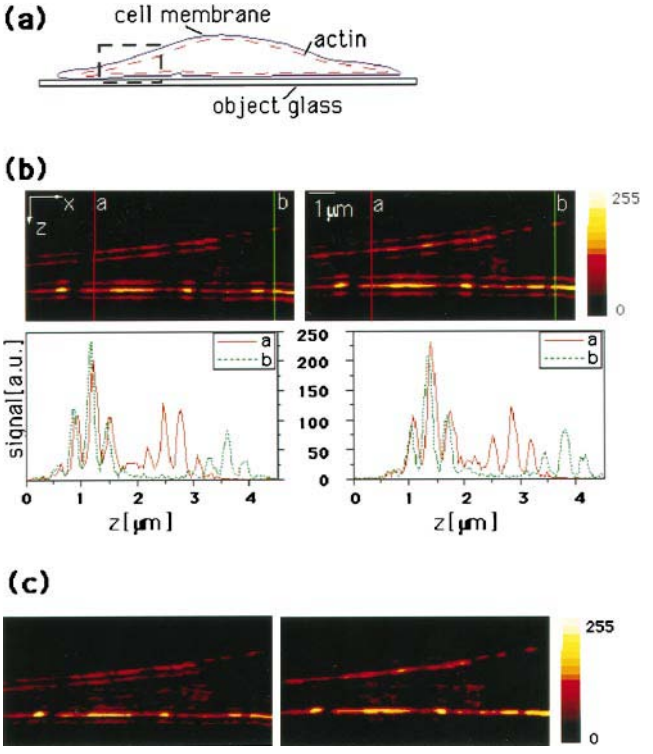

FIGURE 5 An *x-z* image through a fibroblast cell as recorded with a two-photon excitation 4Pi-confocal microscope. (*a*) Sketch indicating the location of the imaged area within the cell. (*b*) Two-photon 4Pi-confocal image without (*left*) and with (*right*) compensation for phase changes induced by a refractive index mismatch. The intensity profiles along the indicated lines show the relative phase of the interfering wavefronts. (*c*) The effect of the point deconvolution for the axial image without (*left*) and with (*right*) phase compensation.

A 4Pi-confocal microscope and two-photon excitation. Two-photon excitation was accomplished with a mode-locked Ti: sapphire laser providing 130-fs pulses at 817 nm. The objective lenses (Leica Planapo; 100×) featured a nominal numerical aperture of 1.4 (oil) that in practice is closer to ~1.35. The fluorescence light was imaged through one of the lenses onto a confocal pinhole that was 65% of the size of the back-projected maximum of the illumination PSF.

Fig. 5 *a* is a sketch of the imaged cell. The image is taken from the area (Fig. 5 *a*) marked with dashes. Actin bundles running close to the membrane are visible; the membrane itself is not, because it was not labeled. The images in Fig. 5 *b* show the data as directly delivered by the detector. This allows the visualization of the lobes and the relative phase of the interfering wavefronts. The lobes render several parallel lines. To further illustrate this effect, we plotted two axial profiles of the fluorescence signal along the marked lines a and b of Fig. 5 *b*. Because the actin bundles are very thin (<100 nm), the profiles represent an axial profile of the 4Pi PSF that is centered at the axial position of the bundle. In the cell, the relative height of the axial lobes is increased with respect to the theoretical case of Fig. 2, which can be attributed to aberrations that are usually encountered in a practical system. Line a in Fig. 5 *b* (*bottom left*) probes the 4Pi-confocal PSF at an axial position of about $z = 1240$ nm and at $z = 2600$ nm. The profile of line b probes the 4Pi PSF at $z = 1240$ nm and $z = 3600$ nm.

The actin fibers are well suited for demonstrating the effect of the refractive index-induced phase change. In the image on the left-hand side of Fig. 5 *b*, the profiles indicate constructive interference at $z = 1240$ nm and $z = 3600$ nm, but destructive interference at $z = 2600$ nm. The lower, horizontal fiber is almost parallel to the focal plane, which is equivalent to a nearly constant value of z. As a result, the relative phase does not change along this fiber. In contrast, the tilted fiber goes upward in z (from the *bottom left* to the *top right*) and therefore experiences a changing relative phase of the interfering spherical wavefronts. Therefore the axial profiles of the tilted fiber illustrate how the relative phase of the wavefronts changes as the sample is scanned along the optic axis.

When evaluating Fig. 5 *b* (*left*) and other similar images, we find that for the glycerol-mounted specimens, an axial movement of ~2.6 μm changed the relative phase by 2π. This is in close agreement with calculations based on a high-aperture focusing theory. As long as the sample thickness is moderate (<30 μm for a glycerol mounted sample), the phase change is a linear function of the axial movement of the sample (Egner et al., 1998). As a result, the phase change induced by the refractive index mismatch can be compensated for by linearly changing the optical path length with a piezoelectrically driven mirror.

The image on the right-hand side of Fig. 5 *b* shows the actively phase compensated counterpart to the image on the left. Compensation was carried out by applying an appropriate voltage ramp to the piezo-driven mirror (Fig. 1) while

scanning axially. The ramp signal was derived from the voltage ramp driving the *z*-piezo of the sample stage. For this purpose we adjusted the amplitude with a voltage divider to ensure proper compensation per axial displacement of the sample. The correct amplitude of the ramp was found by monitoring the signal of axial line scans such as those of lines a and b. The ramp was adjusted until the PSFs in lines a and b were both constructive. The experimentally obtained voltage setting was independently verified by comparing it with the theoretically anticipated value of a 2π change for a 2.6-μm axial scan. The tilted fiber bundle and the corresponding profiles now show that the PSF is constructive throughout the axial image.

To demonstrate the importance of compensation, we applied the point deconvolution to both the compensated and uncompensated images (Fig. 5 *c*). Without active phase compensation, point deconvolution cannot be applied. Whereas the horizontal fiber is properly reproduced, the tilted fiber features ghost structures at certain axial heights. In the phase-compensated image the artifacts are absent, and the tilted fiber bundle can be observed throughout the section with increased axial resolution.

It is clear that refractive index mismatch phase compensation depends only on the numerical aperture of the lenses and on the refractive index of the mounting medium. Once it is established for a certain mountant (here glycerol), it is valid throughout the sample and, of course, in any similarly mounted sample observed with 1.4 nominal aperture oil immersion lenses. Below we show various examples of type A 4Pi-confocal images, all of which were recorded with active phase compensation. Fig. 6 shows a comparison of axial images (*xz* images) as recorded in a different location

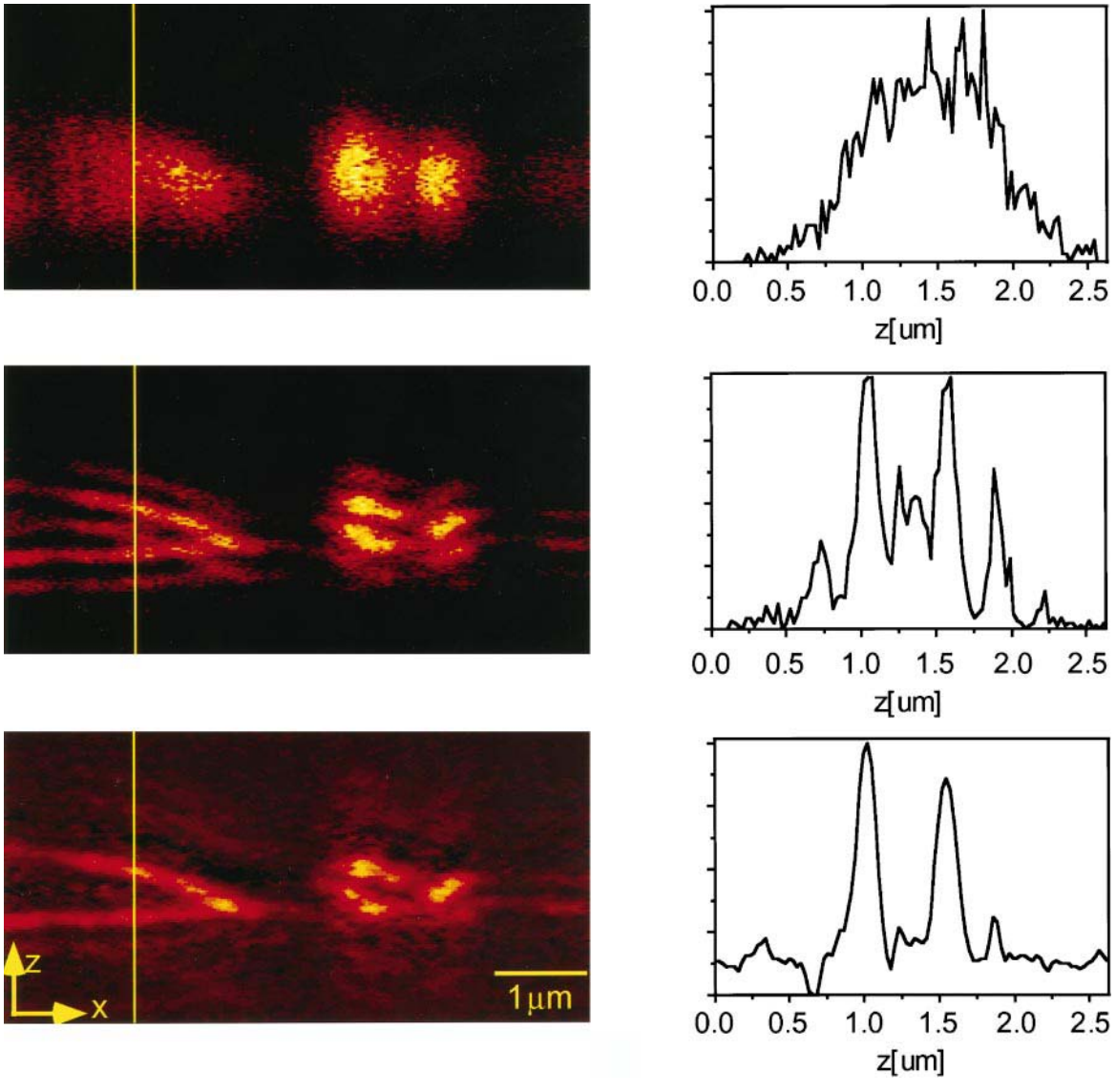

FIGURE 6 *x-z* images similar to those in Fig. 5, but from a different location of the sample: two-photon confocal (*top*), two-photon 4Pi-confocal (*center*), and two-photon 4Pi-confocal after side-lobe removal (*bottom*). The right columns show the intensity profiles along the lines indicated in the respective images.

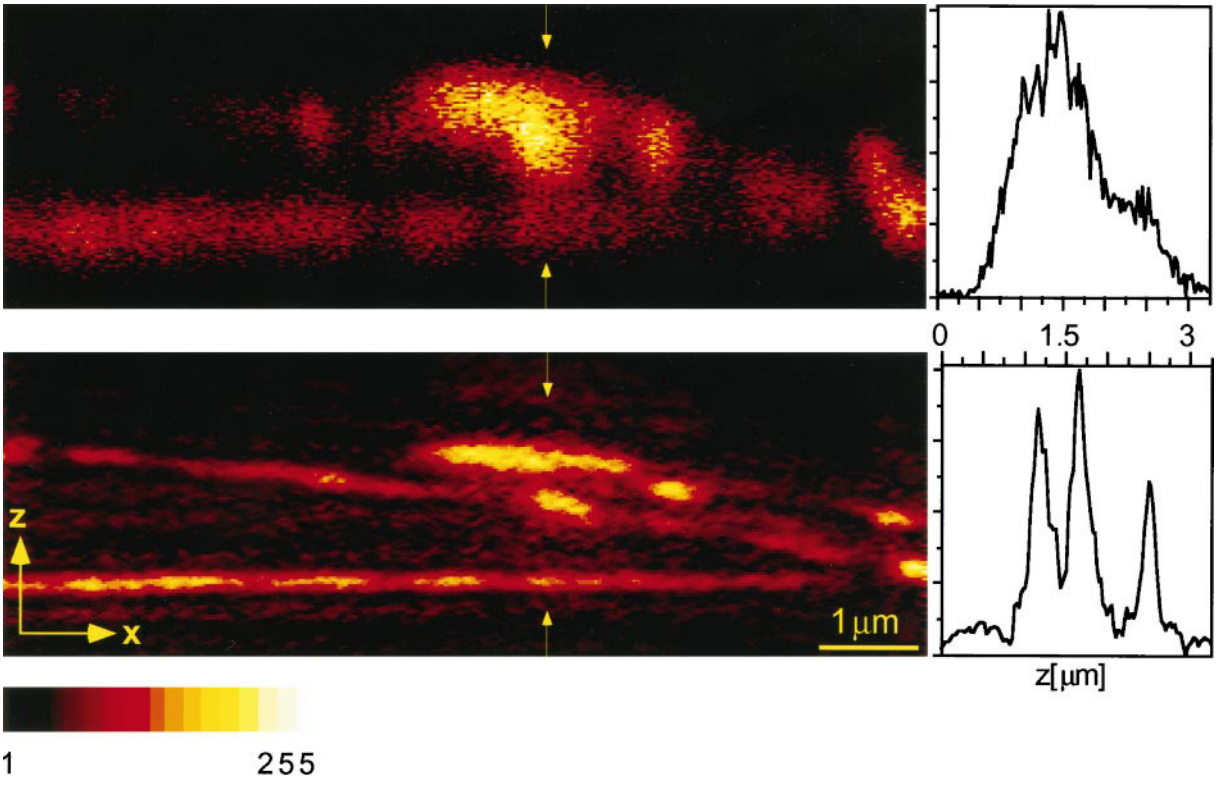

FIGURE 7 Two-photon confocal and two-photon 4Pi-confocal axial image after side-lobe removal through point deconvolution.

in the sample (*top*) in the single lens two-photon confocal microscope and in the two-photon 4Pi-confocal mode (*middle*) before point deconvolution and (*bottom*) after point deconvolution. Because of increased axial resolution, the two-photon 4Pi microscope reveals the junction much better than its two-photon confocal counterpart.

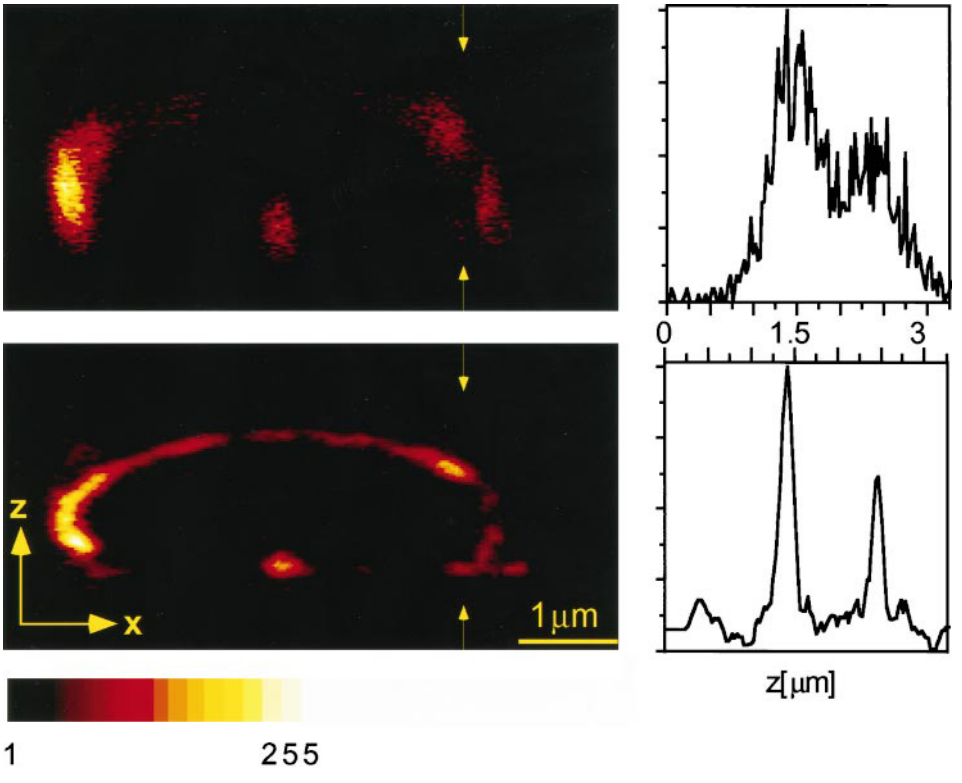

FIGURE 8 Two-photon confocal image and two-photon 4Pi-confocal image after side-lobe removal of a O-ring-shaped structure- showing a higher resolution in the curvature as well as more uniform fluorophore distribution in the 4Pi case.

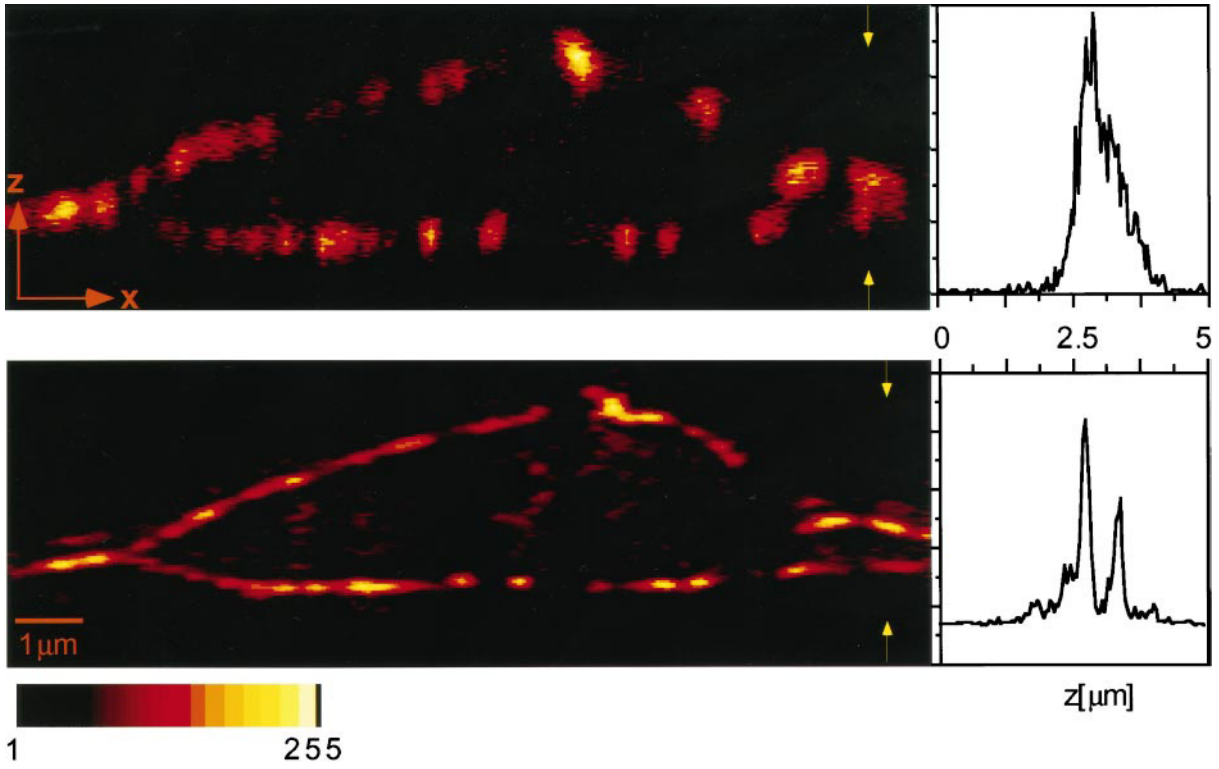

FIGURE 9 Axial image through a fibroblast cell showing an area of ~15 × 5 µm. (*Top*) Two-photon confocal and (*bottom*) two-photon 4Pi-confocal after side-lobe removal.

COLOCALIZATION OF THE FOCUSED ELECTRIC FIELDS

Alignment and tight control of the interfering electric fields is of primary importance in 4Pi-confocal imaging. In this paragraph we give a brief description of the alignment and interferometric matching procedure. When carrying out type A 4Pi-confocal microscopy, it is essential that the two illumination paths are matched within the coherence length of the laser. In the case of two-photon excitation by a mode-locked titanium-sapphire laser, the coherence length is determined by the pulse length (130 fs) and is ~25–30 µm. The optical path length in both illumination arms is adjusted within an accuracy of a few microns by observing interference fringes produced by a reflective sample that is illuminated from both sides with each of the lenses. The interference pattern is observed in the exit of the beamsplitter (Fig. 1) while the beamsplitter and the mirror M_1 are moved parallel to the direction of the incident light. For a path length difference of less than the coherence length of the laser, interference fringes appear.

The confocal pinhole is adjusted by observing the two-photon fluorescence of a solution of rhodamine 6G dissolved in immersion oil. The confocal pinhole also ensures a tight spatial correlation between the illumination spot in the sample and the detector. This tight correlation is helpful for aligning the second objective lens because, if the fluorescence generated by the second lens enters the pinhole, the overlap of the two foci in the sample is automatically given. In our system the second lens is piezoelectrically adjustable with a closed-loop controlled precision of ~10 nm in 3D.

Moreover, with two-photon excitation, equal and coherent illumination of a uniform solution through both objective lenses increases the signal by threefold over that of a single lens at equal total illumination power, provided the focal electric fields overlap perfectly in space (Hänninen and Hell, 1994). This effect is due to the rise in local intensity induced by the interference and the resulting stronger nonlinear fluorescence signal. It is analogous to the threefold signal increase in two-photon-fluorescence-based autocorrelators for ultrashort pulse width determination (Schubert and Wilhelmi, 1986). As a single objective lens provides just half of the total power, the signal increases even sixfold over that induced by a single lens. Along with lobe suppression and high contrast, the signal increase by nonlinear excitation is a sensitive criterion for initial alignment and control of the focal field overlap. Another measure for monitoring and locking the foci is the registration of the transmitted illumination light of path 1 or path 2 by a camera. Thus any changes in the illumination path or any drift of the second objective will be visible and can be counteracted manually or automatically in a closed-loop control.

IMAGES

We applied two-photon excitation 4Pi-confocal microscopy to record three-dimensional images of mouse skin fibroblast cells (Figs. 5–10). All experiments were carried out with oil

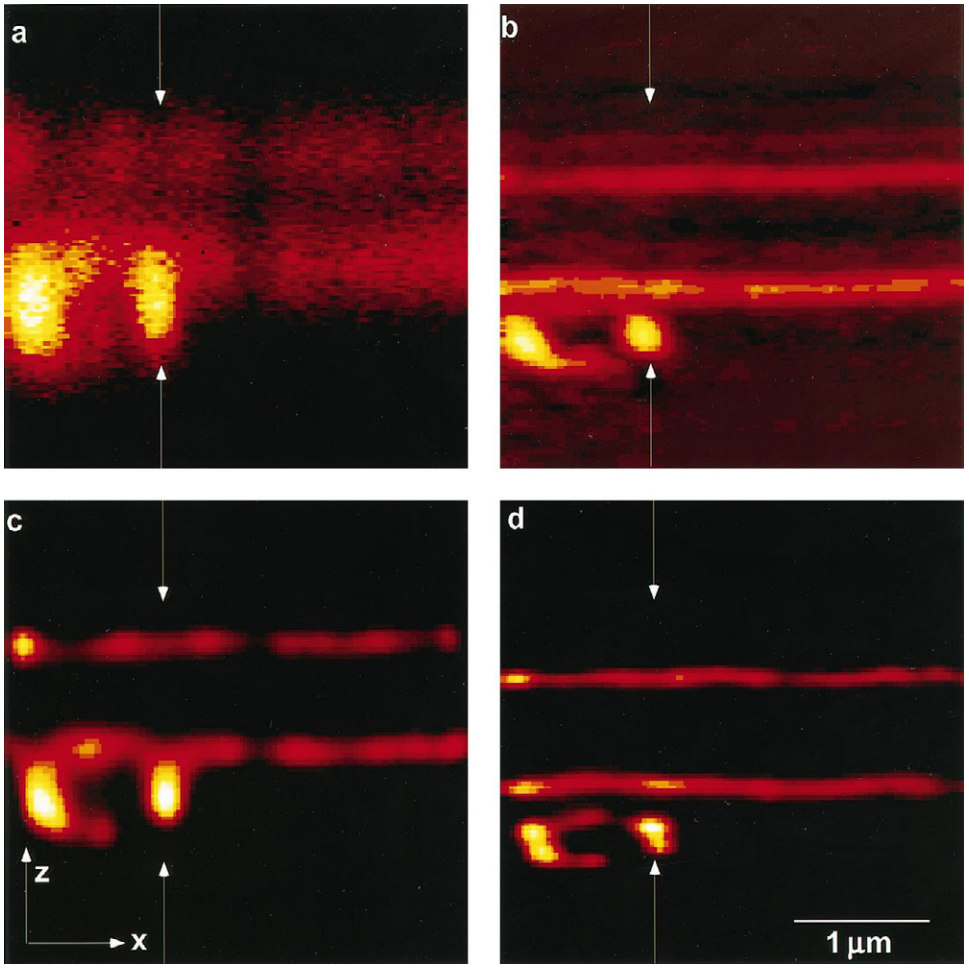

FIGURE 10 Comparison of two-photon excitation. (*a*) Confocal, (*b*) 4Pi-confocal, (*c*) restored confocal, and (*d*) restored 4Pi-confocal image of the same axial section in the fibroblast specimen.

immersion objective lenses (Leica PL APO, 100× NA, 1.4 oil). Pulsed illumination as provided by a mode-locked titanium-sapphire laser was used. The average illumination intensity at the entrance pupil of each lens was ~500 μW. The pixel dwell time was 2 ms, and the pixel size 25 nm in the axial and 50 nm in the lateral directions, respectively. The fluorescence light was filtered by means of a dichroic beamsplitter and by infrared absorbing color glass (2 mm of BG 39; Schott, Mainz, Germany). The detection pinhole in front of our detector was 20 μm, which was ~65% of the back-projected Airy disk diameter. We detected the fluorescence with an avalanche photo diode (SPCM-131-AQ; EG&G Optoelectronics, Vaudreuil, Canada) featuring a specified quantum efficiency of 50–70% in the yellow-red wavelength range. We recorded a series of axial sections that were laterally displaced by 50 nm. The refractive index mismatch-induced phase change was actively compensated for by a linear ramp applied to the piezo-actuated mirror. After recording the two-photon 4Pi-confocal data, we blocked path 2, doubled the intensity in path 1, and recorded a standard two-photon confocal stack for comparison. Doubling the illumination power in path 1 ensured that the two recordings were carried out with the same photon flux.

Fig. 7 displays axial sections in the fibroblast cell as recorded with the standard two-photon confocal (*top*) and with the two-photon 4Pi-confocal configuration using a point deconvolution (*bottom*). The images show a junction of actin bundles. In the 4Pi image the background is slightly higher than in the standard confocal microscope, because of the side-lobe removal algorithm. It eventually stems from noise, small phase fluctuations, or inaccuracies of the inverse lobe function used for point deconvolution. Nevertheless, the 4Pi image reveals the junction of the actin bundles much more clearly than the standard confocal image. It also resolves another fiber bundle on top of the junction that cannot be separated in the confocal image.

The pair of images in Fig. 8 display axial images through actin fiber bundles, arranged in an O-ring fashion. The O-ring shape is more easily recognizable in the 4Pi-confocal image. The comparison reveals some important consequences that are ultimately traced back to the narrower effective focus of the two-photon 4Pi-confocal microscope (250 nm lateral and 140 nm axial). Because of the axially narrower effective PSF, the curvatures are better resolved in the 4Pi-confocal case. Moreover, whereas the axially elongated effective focus of a single-lens (confocal) microscope tends to overemphasize structures parallel to the optic axis (they appear brighter as compared to the rest of the section after normalization), the more spherical spot of the two-

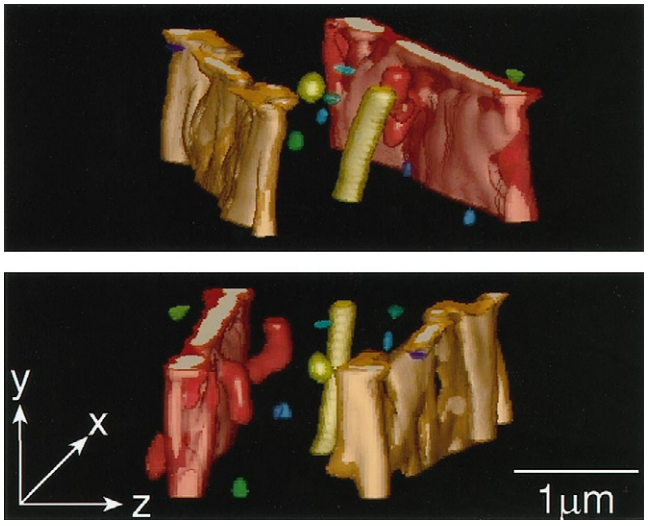

FIGURE 11 Different views of a 3-D data stack recorded with the two-photon 4Pi-confocal microscope. The stack shows a volume of 3.5 × 3.5 × 1 μm within a fibroblast cell containing labeled actin filaments. The data have been restored with the experimental 4Pi-PSF. The rendering shows isosurfaces of 6% (*outer semitransparent structure*) and 22% (*inner opaque structures*). The colors do not represent different intensities, but isolated structures of the isointensity object.

photon 4Pi-confocal microscope gives a much better representation of the fluorophore distribution.

For successful point deconvolution, the assumed height of the lobes has to be carefully selected. If the lobes are chosen too low or too high, the real structure will be accompanied by high background and echoed structures in the deconvoluted image. The example of Fig. 8 shows such residual echoes in the image. However, these effects can be counteracted by ensuring correct initial phase adjustment when the image is recorded. Fig. 9 (*bottom*) displays a 5 × 15 μm axial image through the fibroblast, showing the stability of the 4Pi recording and the point deconvolution across a comparatively large area.

To provide a direct comparison of the resolution between standard two-photon confocal, point-deconvoluted two-photon 4Pi-confocal, and the respective MLE-restored counterparts, we applied MLE restoration to the respective three-dimensional data sets. Fig. 10 displays axial slices of the 3D stack of the two-photon confocal image, the two-photon 4Pi-confocal image after side-lobe removal (Fig. 10 *b*), the restored two-photon confocal image (Fig. 10 *c*), and the restored two-photon 4Pi-confocal image (Fig. 10 *d*), respectively. The comparison of Fig. 10, *a* and *c*, shows that the restoration improves the resolution of standard confocal images. The axial FWHM of the bundles in this image decreased from ~600 nm in the confocal image to 220–300 nm in the restored confocal image. The bundles have a distance of ~360 nm. Interestingly, the restored confocal image cannot resolve the crossing fiber bundles in the area close to the arrow on the left-hand side of the image. However, the structure can be resolved by the two-photon 4Pi-confocal microscope (Fig. 10, *b* and *c*). The point-deconvoluted 4Pi-image (Fig. 10 *b*), with its inherent axial resolution of ~140 nm, resolves these bundles (Fig. 10 *b*). Nevertheless, the restored two-photon 4Pi-confocal image (Fig. 10 *d*) reveals several separate bundles at an axial distance of ~110 nm.

Finally, Fig. 11 shows two different views of a restored volume-rendered 3-D data stack of a two-photon 4Pi-confocal microscope. The rendering shows isosurfaces of 6% (outer semitransparent structure) and 22% (inner opaque structures). The colors do not represent different intensities, but isolated structures of the isointensity object. The volume of 3.5 × 3.5 × 1 μm shows a very dense layer of actin filaments on the inside of the cell membrane (*red and brown layers*), a fiber bundle in the center, and two other bundles reaching from the bottom layer (*red*) into the cell. The data show the applicability of two-photon 4Pi-confocal microscopy to imaging the actin structure in the cell with a 3D resolution of ~180–210 nm in the lateral direction and 80–100 nm in the axial direction.

DISCUSSION AND CONCLUSION

So far, two concepts promise fundamentally increased axial resolution: standing-wave microscopy (SWM) and 4Pi microscopy. The sharp interference maxima of the SWM provide 50–120-nm fine layers of excitatory light that allow structures as close as 50–200 nm to be discerned. However, with thicker objects the periodicity of the maxima has to be taken into account. The same applies to more recent, related, and similarly promising approaches using conventional illumination (Gustafsson et al., 1997). Based on conventional microscopy, standing-wave concepts lack an intrinsic axial resolution. Featuring several excitation and detection layers of almost equal intensity, the lobes pose high demands on the restoration procedures for obtaining unambiguous 3D imaging. The concept of 4Pi-confocal microscopy aims at achieving a superresolving PSF that is three-dimensionally confined. To achieve this goal we focus wavefronts of high numerical aperture, employ two-photon excitation of the fluorophore, and detect confocally in a scanning arrangement. Compared to the SWM, the two-photon 4Pi-confocal microscope features a larger axial FWHM, because of the doubled excitation wavelength and high-aperture focusing. However, these measures allow us to reduce the lobes and to obtain a three-dimensionally confined PSF, which are paramount conditions for fast and stable point deconvolution. The latter renders an axially sharper image in 3D microscopy, even in thicker biological specimens.

The active axial phase compensation cancels out phase changes that are induced by the refractive index mismatch between the medium and the mounting medium, but not putative random phase changes caused by changes in the refractive index in the cell cytoskeleton. Importantly, our 4Pi images reveal that the phase between the interfering wavefronts does not change randomly during scanning. So far we have not observed phase jumps caused by sudden

changes in the refractive index. Even for 10–15-μm images, such as those of Figs. 5, 7, and 10, the relative phase of the wavefronts remained constant at a given axial position of the focus (see the horizontal fibers running parallel to the focal plane). If the material above and below had caused a firm change in the relative phase, this change would have been manifested in the fiber image. We think this is because in the mounted cell outside the nucleus, the glycerol largely dominates the index of refraction. Small changes in refractive index as induced by small organelles might induce "dents" in the converging spherical wavefront. However, the phase at the focal point is given by coherent summation across the whole converging wavefront, which mostly encounters glycerol. Small random "dents" are expected to be averaged out at the focal point, so that the glycerol part of the wavefront dominates the resulting phase in the focal point. Our experimental observation supports this expectation. The phase effect of the glycerol can be accounted for in the active phase compensation procedure, so that two-photon 4Pi-confocal microscopy becomes applicable at least in the cytoskeleton of a fixed cell, and even for comparatively large areas of more than 15 μm. Our results encourage us to concentrate further investigations of 4Pi imaging on the nucleus, where more sudden changes in the phase might be expected. In our view, the 3D confinement of the two-photon 4Pi-confocal PSF and the relatively low lobes make these experiments a realistic endeavor.

In conclusion, we demonstrated three-dimensional two-photon 4Pi-confocal imaging of fluorescently labeled actin fiber bundles of a glycerol-mounted fibroblast cell with an axial resolution that is three to four times better than that of a two-photon confocal microscope. The axial resolution of $\sim$145 nm (FWHM) surpasses its lateral counterpart of 250 nm.

The superresolution in the z direction is a direct consequence of the fact that the two spherical wavefronts provide superior coverage of the aperture along the optic axis. In this paper, we showed the applicability of a fast point deconvolution algorithm for achieving defined axial resolution in the cytoskeleton. In addition, we described stringent alignment procedures and experimentally demonstrated how to overcome the effect of refractive index mismatch-induced phase changes. Powerful off-line image restoration can further improve the 3D resolution, but in two-photon 4Pi-confocal microscopy extensive restoration is not required to remove lobes and to achieve axial superresolution.

The authors express their thanks to H. T. M. van der Voort for performing the image restoration in Figs. 10 and 11 (the restoration was performed with the Huygens restoration software from Scientific Volume Imaging (SVI), Hilversum, The Netherlands), to H.-M. von Stockhausen for the isosurface presentation of Fig. 11 (the rendering of Fig. 11 was done using 3D-Tool, developed at the MPI for Neurological Research, Köln, Germany), and to M. Gilbert for technical assistance in fibroblast sample preparation.

KB is supported by the Deutsche Forschungsgemeinschaft through a grant to SWH (He-1977).

REFERENCES

Agard, D. A., and J. W. Sedat. 1983. Three-dimensional architecture of a polytene nucleus. *Nature.* 302:676–681.

Bacallao, R., M. Bomsel, E. Stelzer, and J. de Mey. 1990. Guiding principles of specimen preservation for confocal fluorescence microscopy. *In* Handbook of Biological Confocal Microscopy. Plenum Press, New York. 197–205.

Bailey, B., D. L. Farkas, D. L. Taylor, and F. Lanni. 1993. Enhancement of axial resolution in fluorescence microscopy by standing-wave excitation. *Nature.* 366:44–48.

Carrington, W. A., R. M. Lynch, E. D. W. Moore, G. Isenberg, K. E. Fogarty, and F. S. Fay. 1995. Superresolution in three-dimensional images of fluorescence in cells with minimal light exposure. *Science.* 268:1483–1487.

Egner, A., M. Schrader, and S. W. Hell. 1998. Refractive index mismatch induced intensity and phase variations in fluorescence confocal, multiphoton and 4Pi-microscopy. *Opt. Commun.* 153:211–217.

Freimann, R., S. Pentz, and H. Hörler. 1997. Development of a standing-wave fluorescence microscope with high nodal plane flatness. *J. Microsc.* 187:193–200.

Gu, M., and C. J. R. Sheppard. 1994. Three-dimensional transfer functions in 4Pi confocal microscopes. *J. Opt. Soc. Am. A.* 11:1619–1627.

Gustafsson, M. G. L., D. A. Agard, and J. W. Sedat. 1995. Sevenfold improvement of axial resolution in 3D widefield microscopy using two objective lenses. *Proc. SPIE.* 2412:147–156.

Hänninen, P. E., and S. W. Hell. 1994. Femtosecond pulse broadening in the focal region of a two-photon fluorescence microscope. *Bioimaging.* 2:117–122.

Hänninen, P. E., S. W. Hell, J. Salo, E. Soini, and C. Cremer. 1995. Two-photon excitation 4pi confocal microscope: enhanced axial resolution microscope for biological research. *App. Phys. Lett.* 66:1698–1700.

Hell, S. W., S. Lindek, and E. H. K. Stelzer. 1994. Enhancing the axial resolution in far-field light microscopy: two-photon excitation 4Pi-confocal fluorescence microscopy. *J. Mod. Opt.* 41:675–681.

Hell, S., and E. H. K. Stelzer. 1992. Fundamental improvement of resolution with a 4Pi-confocal fluorescence microscope using two-photon excitation. *Opt. Commun.* 93:277–282.

Hell, S., and E. H. K. Stelzer. 1992. Properties of a 4Pi-confocal fluorescence microscope. *J. Opt. Soc. Am. A.* 9:2159–2166.

Hell, S. W., M. Schrader, and H. T. M. van der Voort. 1997. Far-field fluorescence microscopy with three-dimensional resolution in the 100 nm range. *J. Microsc.* 185:1–5.

Kano, H., H. T. M. van der Voort, M. Schrader, G. M. P. van Kempen, and S. W. Hell. 1996. Avalanche photodiode detection with object scanning and image restoration provides 2–4 fold resolution increase in two-photon fluorescence microscopy. *Bioimaging.* 4:187–197.

Lanni, F. 1986. Applications of Fluorescence in the Biological Sciences. Liss, New York.

Lindek, S., N. Salmon, C. Cremer, and E. H. K. Stelzer. 1994. Theta microscopy allows phase regulation in 4Pi(A)-confocal two-photon fluorescence microscopy. *Optik.* 98:15–20.

Loew, L. M., R. A. Tuft, W. Carrington, and F. S. Fay. 1993. Imaging in five dimensions: time-dependent membrane potentials in individual mitochondria. *Biophys. J.* 65:2396–2407.

Pawley, J. 1995. Handbook of Biological Confocal Microscopy. Plenum Press, New York.

Schrader, M., and S. W. Hell. 1996. 4Pi-confocal images with axial superresolution. *J. Microsc.* 183:189–193.

Schubert, M., and B. Wilhelmi. 1986. Nonlinear Optics and Quantum Electronics. John Wiley and Sons, New York.

Sheppard, C. J. R., and D. M. Shotton. 1997. Confocal Laser Scanning Microscopy. Bios Scientific Publishers, Oxford.

Van der Voort, H. T. M., and K. C. Strasters. 1995. Restoration of confocal images for quantitative analysis. *J. Microsc.* 178:165–181.

Wilson, T., and C. J. R. Sheppard. 1984. Theory and Practice of Scanning Optical Microscopy. Academic Press, New York.